

# Simulative and Experimental Determination of the Tooth Flank Fracture Load Capacity of Large Modulus Gears

Christian Brecher, Christoph Löpenhaus and Fabian Goergen

## 1. Introduction and Motivation

Because of continuously increasing power density in modern transmissions, the damage pattern tooth flank fracture (TFF) is becoming a limiting factor in terms of gearbox lifetime. Tooth flank fractures depend on numerous influencing parameters. On the one hand contact pressure influences as well as influences of bending, shearing and compression downstream of the Hertzian contact exist. In addition, residual stresses are superimposed on the time-variable load stresses, which can even manifest themselves in the form of tensile residual stresses in the volume critical for tooth flank fracture. On the other hand, the local material properties have a significant influence on the development of tooth flank fractures, since the crack initiation under the surface takes place in the area of low local hardness and preferably at material inhomogeneities (e.g. voids, non-metallic inclusions, carbides). In recent years, numerous calculation methods have been developed to estimate the tooth flank fracture load capacity and been validated on several gear geometries. However, discrepancies frequently occur in the calculation of the tooth flank fracture load capacity, especially for large-modulus helical gears from industrial practice. One

possible reason is that the validation is usually based on experimental results from research environment. The experimental investigation of large-modulus helical gears from industrial practice is not economically feasible, which is why smaller gears are used. For this reason, there is currently no generally applicable calculation approach for determining the tooth flank fracture load capacity.

Two research motivations result from the current deficits. On the one hand, a generally valid calculation approach has to be developed for the determination of the tooth flank fracture load capacity, which has been validated both on gears from the research environment and on large-modulus gears from industrial practice. The validation requires statistically verified experimental results which cannot be determined economically for large-modulus helical gears from industrial practice. For this reason, an analogy test has to be developed which enables the economic determination of the tooth flank fracture load capacity of gears from industrial practice on the other hand.

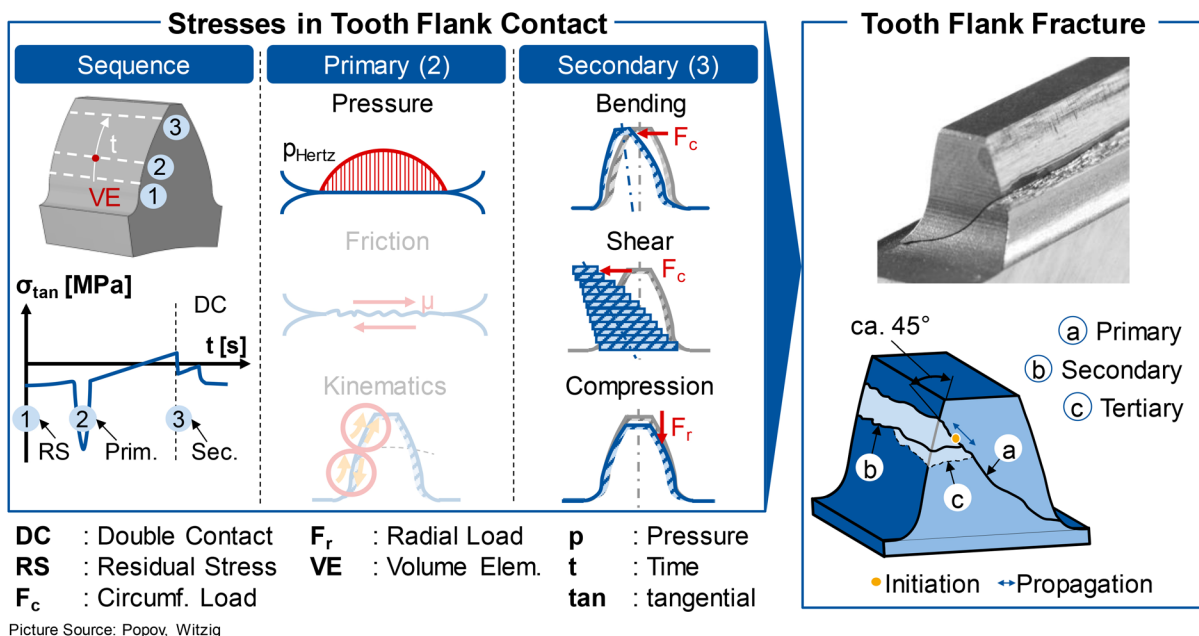


Figure 1 Stresses in Tooth Flank Contact and Tooth Flank Fracture [Ref. POPO 10, Ref. WITZ, Ref.12].

© WZL

## 2. Tooth Flank Fracture in the State of the Art

The processing of the damage type tooth flank fracture in the state of the art takes place in three steps. In the first step, the stresses in tooth flank contact are explained and their relevance for the development of tooth flank fractures is evaluated. Subsequently, the method for the TFF load capacity calculation according to KONOWALCZYK is presented [Ref. KONO18]. Finally, the concept developed by KONOWALCZYK for the investigation of tooth flank fractures is presented in an analogy test [Ref. KONO18].

### 2.1 Stresses in Tooth Flank Contact

The loading of a volume element which is located on or below the tooth flank surface can be characterized in three steps, Figure 1. If no external load is present, then a constant residual stress-state, step 1, prevails in the volume element. In the active tooth flank contact, as a result of the HERTZIAN contact flattening, mechanical compressive stresses predominantly build up in the volume element which are superimposed on the residual stress-state, Figure 1 [Ref. LOEP15]. The stress state immediately below the HERTZIAN contact zone is determined by normal, tangential and temperature stresses due to friction, slippage, micro and macro HERTZIAN contact [Ref. LOEP15]. In higher material depths, the influence of the macro HERTZIAN contact is dominant and the tribological influencing factors are assumed to be negligibly small [Ref. ANNA03].

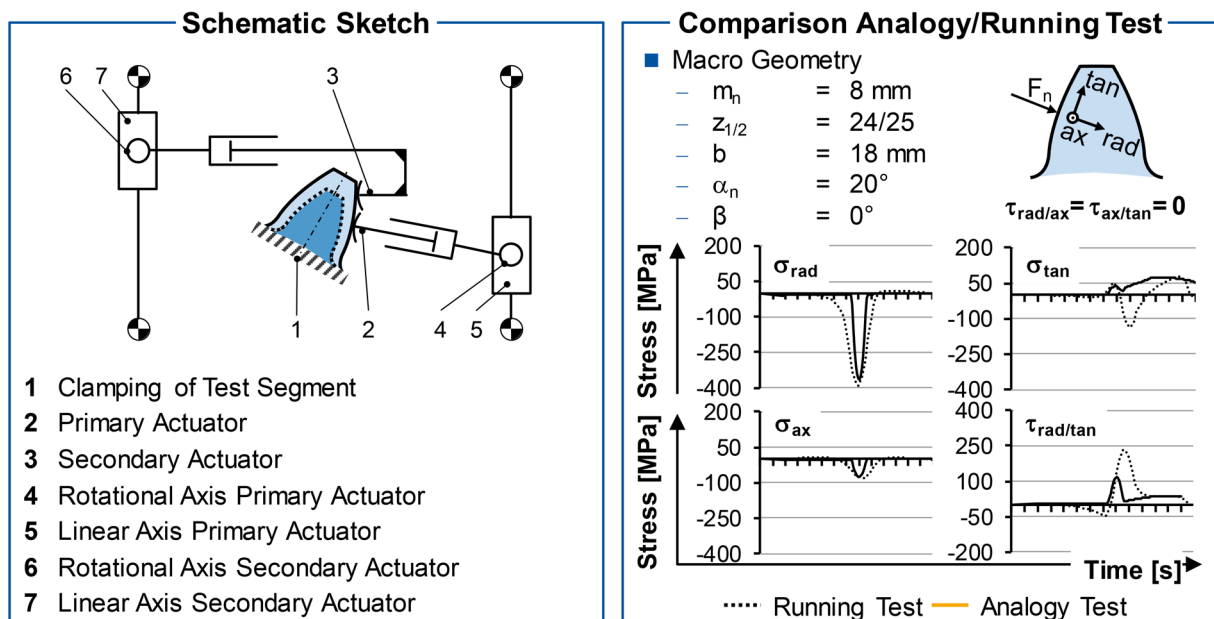
After the HERTZIAN contact the volume element is stressed as a consequence of tooth deformation. Tensile normal and shear stresses build up, which increase until the change to multiple tooth meshing due to the increasing lever arm, Figure 1 [Ref. LOEP15]. The tooth flank fracture has its initial crack location under the surface at a depth of  $t \approx 2 \cdot \text{CHD}_{50}$ , preferably at a material inhomogeneity (e.g. void, non-metallic inclusion, carbide). According to the current state of knowledge, the cause of the crack initiation is assumed to be a stress increase due to the

modulus of elasticity difference between the inhomogeneity and the microstructure as well as the notch effect of the inhomogeneity [Ref. WITZ12].

The damage type tooth flank fracture is therefore significantly influenced by HERTZIAN contact pressure in combination with secondary mechanical stresses (bending, shear, compression) [Ref. BRUC06, Ref. WITZ12, Ref. KONO18]. Compared to the stress condition of the tooth flank near the surface ( $0 \text{ mm} \leq t \leq t_{\text{vonMises,max}}$ ), the stresses in the tooth flank fracture critical area are low and the influence of the low material strength predominates [BRUC06]. The low local strength is a result of the transition between hardened surface layer and unhardened core structure, which results in a locally low hardness in combination with low compressive residual stresses or even tensile residual stresses [Ref. KONO18].

### 2.2 Calculation of Tooth Flank Fracture Load Capacity

In recent years, numerous calculation methods have been developed to determine the tooth flank fracture load capacity [Ref. WEBE15, Ref. PATE16, Ref. WICK17, Ref. OCTR18, Ref. LEIM19, Ref. MEIS19]. The calculation methods have in common that the local safety or material strain is determined in the form of a comparison between local stress and stress resistance, whereby the determination of stress and stress resistance differs in all methods. Especially for large-modulus helical gears all approaches have deficits in order to take all important influencing parameters into account. [Ref. WITZ12, Ref. WICK17, Ref. OCTR18, Ref. LEIM19, Ref. ISO19] use an analytical approach based on the half space theory to calculate the stress sequence which results from the HERTZIAN contact. This approach is not considering tensile stresses which appear before and after the compressive stress peak in high material depth and lead to an alternating load. Furthermore tensile residual stresses in high material depth due to the case hardening process are not considered in [Ref. WITZ12, Ref. WICK17, Ref. LEIM19,



© WZL

Figure 2 Analogy Concept to Investigate the Tooth Flank Fracture Load Capacity.

Ref. ISO19]. Secondary stresses after the HERTZIAN contact flattening in the form of bending, shear and compression are not considered in [Ref. OCTR18, Ref. ISO19]. Other approaches such as [Ref. WITZ12, (Ref. [Ref. WEBE15, Ref. WICK17] use an analytical approach based on the bending beam theory or elastic wedge theory to determine secondary stresses. In this case the analyzed gear is cut into several parts in lead direction and the stress sequence after the HERTZIAN contact flattening is calculated for each segment. In this case cross influences in lead direction are assumed to be negligible small which results in deviations especially for helical gears. Regarding the stress resistance calculation several approaches use empirical factors or nominal strength values from literature or experimental experience which are not considering material inhomogeneities and their statistical distribution [Ref. WITZ12, Ref. PATE16, Ref. OCTR18].

### 2.3 Experimental Investigation of Tooth Flank Fractures in Analogy Tests

KONOWALCZYK shows by simulation of a large-modulus spur gear from research environment that the local material strain in the TFF critical volume can be approximated using a pulsator with two actuators. For this purpose, an analogy concept is developed in which a tooth segment of the test gear is separated by means of electrical discharge machining (EDM) and clamped in a test setup, Figure 2 [Ref. KONO18].

The primary stress is applied by an actuator, which is fixed on the tooth flank above the expected crack origin. To apply the secondary stress, an additional actuator is positioned in the area of the tooth tip. By using two actuators, the new test rig concept differs fundamentally from pulsators for the investigation of tooth root load capacity. The results of the contact simulations carried out in running and analogy tests show the suitability of the test rig concept for the investigation of tooth flank fractures in analogy tests. In particular, the maximum compressive

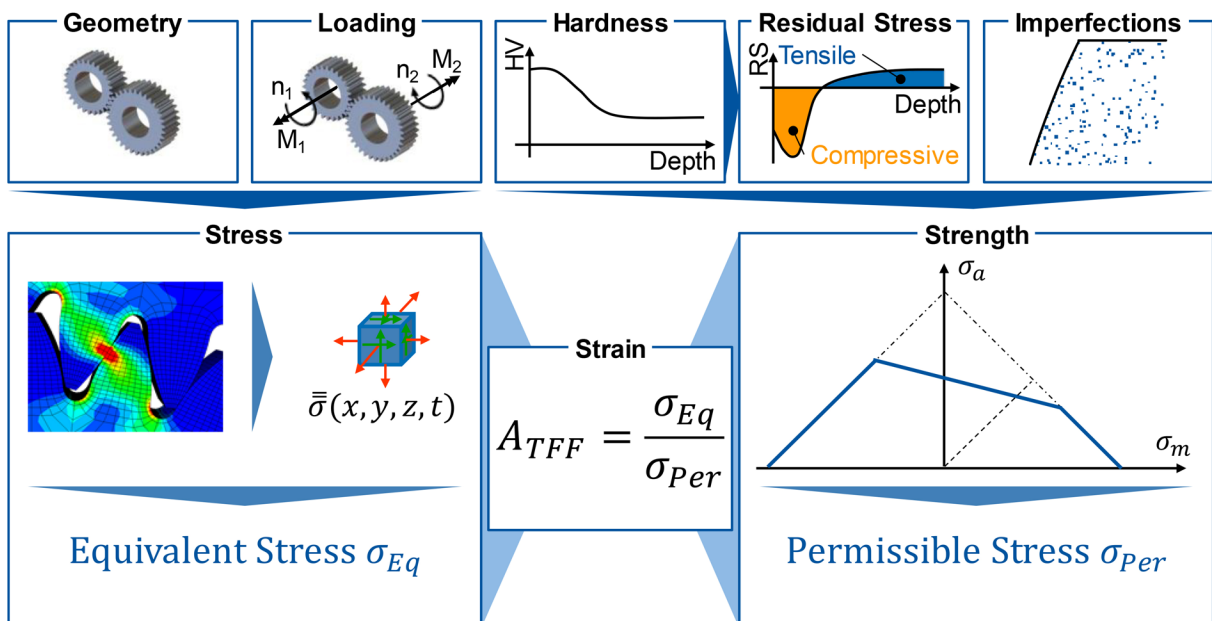
stresses in radial and axial direction (Fig. 2:  $\sigma_{rad}$ ,  $\sigma_{ax}$ ) as a result of the HERTZIAN contact flattening can be accurately mapped by the primary actuator. The tensile stress in tangential direction can also be accurately reproduced by applying the load to the secondary actuator with a time delay to the primary actuator (Fig. 2:  $\sigma_{tan} \geq 0$ ). In this way, the bending stress downstream of the rolling-sliding contact due to tooth deformation is applied. Nevertheless the developed methodology for determining the required pulsator loads only reproduces the maximum amplitudes of the normal stresses sufficiently, but not the stress tensor sequences. Furthermore, the compressive stress in the tangential direction as well as the shear stress in the radial/tangential plane cannot be reproduced sufficiently (Fig. 2:  $\sigma_{tan} < 0$ ,  $\tau_{rad/tan}$ ). With the procedure shown KONOWALCZYK can achieve a correlation of the equivalent stress in the tooth flank fracture critical volume between analogy and running test for the analyzed gear. The investigated gear is an established large-modulus spur gear from the research environment ( $m_n = 8$  mm,  $z_{\frac{1}{2}} = 24/25$ ). [Ref. KONO18]

### 3. Research Aim

The state of the art shows that there is currently no suitable method to determine the tooth flank fracture load capacity by taking all relevant influencing parameters into account. When developing a suitable method for the calculation of the tooth flank fracture load capacity, the following aspects have to be considered in particular:

- FE calculation of the load stresses for the sufficient evaluation of the stress state
- Consideration of possible tensile residual stresses in higher material depth
- Consideration of material inhomogeneities in the microstructure

For the experimental validation of the method on large-modulus helical gears from industrial practice, a suitable analogy



© WZL

Figure 3 Calculation of TFF Load Capacity according to KONOWALCZYK [Ref. KONO18].

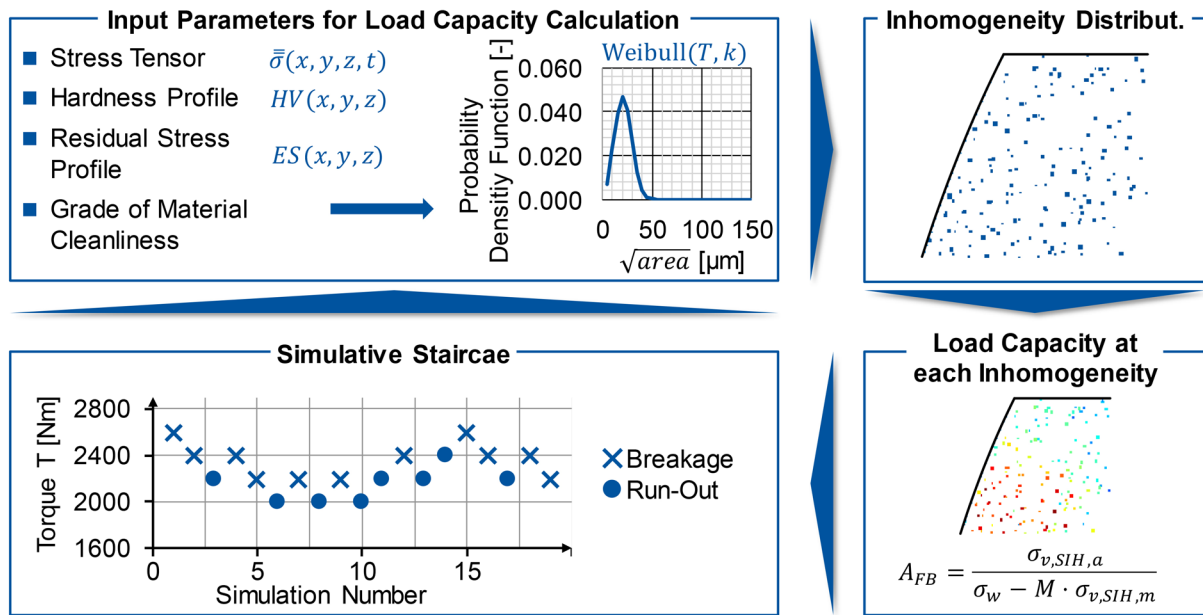


Figure 4 Calculation of TFF Load Capacity according to KONOWALCZYK [Ref. KONO18].

© WZL

concept is also required, as such gears cannot be investigated economically with regard to load capacity in the running test.

The following objective is derived from the existing deficits: *Method for the calculation of the tooth flank fracture load capacity as well as an economic analogy test concept for the experimental investigation of the tooth flank fracture load capacity of large-modulus spur and helical gears.*

In order to achieve the objective, a three-step procedure is chosen. In the first step, the method development taking into account all relevant influencing parameters is done. The method for the calculation of the tooth flank fracture load capacity presented in chapter 4 was developed at WZL and is based on the work of KONOWALCZYK [Ref. KONO18]. Subsequently, the validation of the method takes place based on experimental investigations of a large-modulus spur gear from the research environment. The experimental investigations presented in this report were carried out within the framework of the research project FVA 695 [Ref. KLOC18] and are also based on the work of KONOWALCZYK [Ref. KONO18]. Furthermore, a validation is carried out on the basis of a tooth flank fracture critical large-modulus helical gear from the gearbox of a wind turbine. In the last step, a concept is developed which allows to test the tooth flank fracture load capacity of large modulus helical gears economically in an analogy test as well as a calculation approach to determine the pulsator load-sequences in order to get the same stress-state in the tooth flank fracture critical volume.

#### 4. Calculation Method to Determine the TFF Load Capacity

methods because the stress calculation is 3D-FE-based over the entire mesh cycle, tensile residual stresses in the transition area between surface layer and core hardness can be taken into account and a material inhomogeneity-based, statistical approach serves as a basis for the local strength calculation. The calculation approach is based on the principle of local

endurance strength by The The calculation method described in this report was developed at WZL by KONOWALCZYK and serves as a basis to investigate the tooth flank fracture load capacity at WZL and the current DFG research project BR 2905/90 1 for the reproduction of the damage type tooth flank fracture in an analogy test [Ref. KONO18]. The methodology differs from existing determining the local material strain in every discrete tooth volume element, cf. Figure 3 [Ref. KONO18].

To calculate the equivalent stress, time-dependent stress tensors are determined by a quasistatic simulation of the tooth contact in FEA. The combination to an equivalent stress  $\sigma_{Eq}$ , which considers the time dependency and the rotation of the main stress coordinate system in the rolling-sliding contact, is carried out using a modified variant of the stress intensity hypothesis (SIH) according to LIU [Ref. LIU91, Ref. KONO18]. The determination of the local strength  $\sigma_{Per}$  is based on the calculation of the local alternating strength at material inhomogeneities in the interior of the component according to MURAKAMI [Ref. MURA02]. The statistical distribution of the material inhomogeneities in the tooth volume is carried out according to HENSER [Ref. HENS15]. To determine the local residual stress-state, an optimization algorithm is developed on the basis of a stress equilibrium between compressive and tensile residual stresses. The calculation of compressive residual stresses up to  $t = 0.5 \cdot CHD_{550}$  is realized according to LANG [Ref. LANG79]. Afterwards a continuous transition (equal residual stress value and equal slope) is defined as a first and second boundary condition. The third and fourth boundary conditions are defined by the maximum depth in the tooth center, where the residual stress has to reach a constant value ( $\sigma_{RS,t(max)} \geq 0 \text{ MPa}$ ,  $\sigma'_{RS,t(max)} = 0$ ). The calculated local residual stress value is taken into account by using the mean-stress sensitivity according to the FKM guideline [Ref. FKM03]. The statistical distribution of inhomogeneities leads to different results for each

individual calculation and thus enables the implementation of a simulative staircase method which can be evaluated according to the IABG method, Figure 4 [Ref.HÜCK83]. A statistical distribution of inhomogeneities in the tooth volume is generated in successive calculation steps. The distribution follows a density function, which results from the cleanliness of the material and is described by the scale parameter T and shape parameter k of a Weibull distribution as well as a reference number of the inhomogeneities present in the volume. According to HENSER, this density function is derived from existing fracture surfaces and the inhomogeneities detected by SEM [Ref.HENS15]. On the basis of the locally available data regarding stress, hardness and residual stress condition, it is possible to calculate whether the local strength is exceeded at each inhomogeneity.

The alternating strength  $\sigma_w$  of an inhomogeneity is calculated according to Equation (4-1), whereby no influence of the local mean stresses on the tolerable amplitude is taken into account initially.

$$\sigma_w = 1.56 \frac{HV + 120}{\sqrt[12]{area}} \quad (4-1)$$

$\sigma_w$  Alternating Strength  
 $\sqrt{area}$  Murakami Factor  
 HV Vickers Hardness

This is done in a second step according to MURAKAMI'S recommendation by calculating a mean stress sensitivity M [Ref.MURA02]. In this report the procedure according to FKM is applied for the calculation of the mean stress sensitivity M [Ref.FKM03]. Both load and residual stress induced mean stress components are taken into account. On the basis of the local strain calculation at each inhomogeneity in the tooth volume, the result of a calculation step is evaluated either as a breakage or as a run-out and classified in a simulative staircase procedure (Fig. 4, bottom left). Based on the result, the load for the next

calculation step is defined and the calculation of the load capacity is repeated. The described procedure is repeated a total of 30 to 50 times, so that a high statistical assurance of the result regarding mean value and scatter is available.

## 5. Validation of TFF Calculation Approach

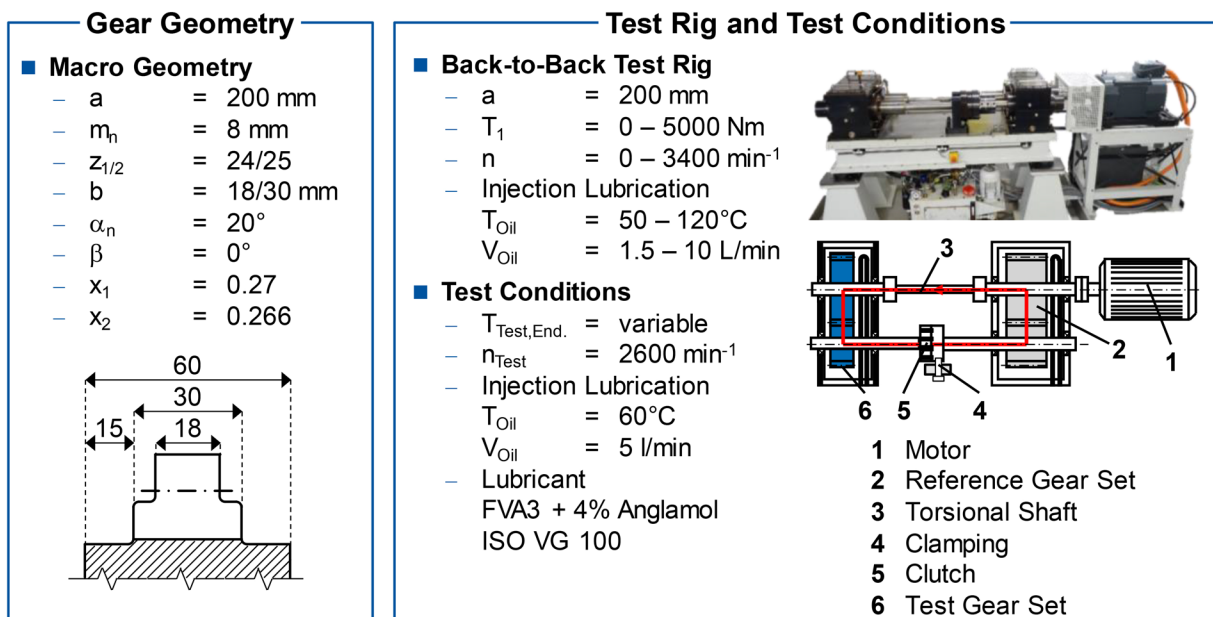
Chapter 5 deals with the experimental validation of the calculation approach described in Chapter 4. The validation is carried out in two steps. First, a large-modulus tooth flank fracture critical spur gear is tested in a back-to-back test rig by means of endurance limit derivation regarding tooth flank fracture in a staircase method. In a second step, a large-modulus helical gear from a wind turbine, which showed several tooth flank fractures in field, is analyzed simulative and compared to the nominal torque during operation.

### 5.1 Experimental Investigation on Back-to-Back Test Rig

The investigations carried out in the present work were carried out on a back-to-back test rig with center distance  $a = 200$  mm. In chapter 5.1.1 the test geometry, the test rig and the test conditions are presented. Chapter 5.1.2 shows the results of the experimental investigations and the comparison to the results of the tooth flank fracture load capacity calculation.

#### 5.1.1. Test Parts, Test Rig and Test Conditions

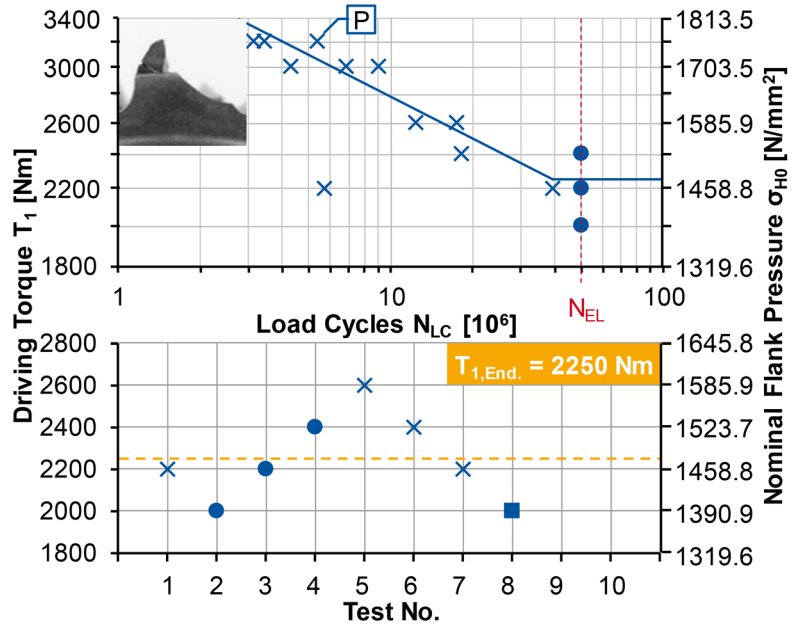
The test gear geometry was determined based on the test variant EHTA out of TOBIE'S work, Figure 5 [Ref.TOBIO1]. The geometry was designed for a center distance  $a = 200$  mm. The main features of the spur gears are a normal module  $m_n = 8$  mm, number of teeth on pinion and gear  $z_{1/2} = 24/25$ , pressure angle  $\alpha_n = 20^\circ$  and profile shift coefficients  $x_{1/2} = 0.27/0.266$ . To avoid premature tooth meshing, a short tip relief with  $C_\alpha = 75 \mu\text{m}$  is applied. The tip relief definition is based on a FE-based penetration calculation [Ref.KONO18]. To minimize edge effects, a low



© WZL

Figure 5 Gear Geometry, Test Rig and Test Conditions.

- **Macro Geometry**
    - $m_n$  = 8 mm
    - $z_{1/2}$  = 24/25
    - $b$  = 18/30 mm
    - $\alpha_n$  = 20°
    - $x_{1/2}$  = 0.27/0.266
  - **Micro Geometry**
    - $C_{\alpha a}$  = 75±5 μm
    - $C_{\beta I, II}$  = 10/10 μm
    - $C_{L, II}$  = 1.8 mm
- 
- × Breakage
  - Run Out
  - Fictitious Point
  - P: Pitting EL: Endurance Limit



© WZL

Figure 6 Experimental Endurance Limit (EL), SN-Curve [Ref. KLOC18].

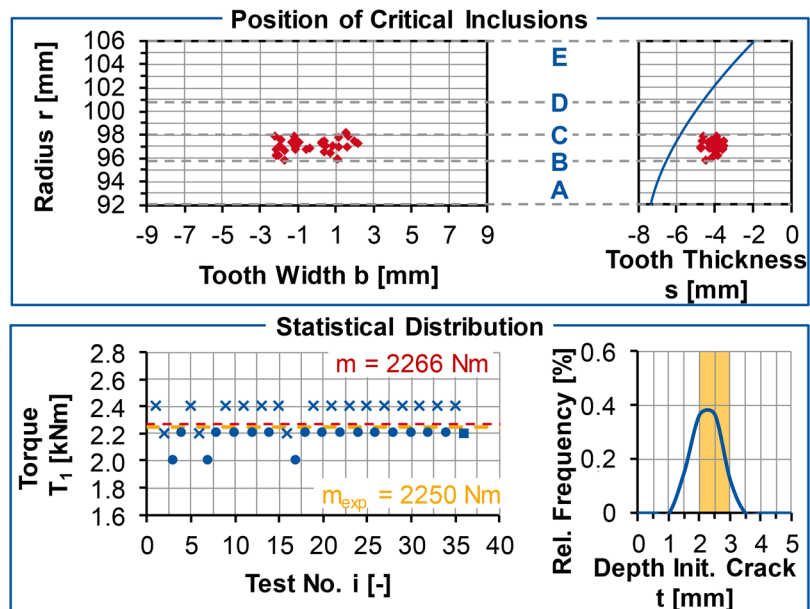
lead crowning of  $C_\beta = 2 \mu\text{m}$  is applied. The distribution of material inhomogeneities was determined according to the method of BRECHER ET AL. [Ref. BREC17]. Therefore single tooth segments were cut in an angle of 45° to the flank surface and the cross section view was captured by light microscopy. To evaluate the defect distribution the automatic algorithm creates cluster of black pixel, which represent material inhomogeneities, in the microscopic picture and evaluates the size of each defect.

The principle of the test rig used corresponds to a standard back-to-back test rig consisting of a motor, a reference gear set and a test gear set, a torsional shaft, a coupling and a clamping,

Fig. 5. The performance data of the test rig enables the

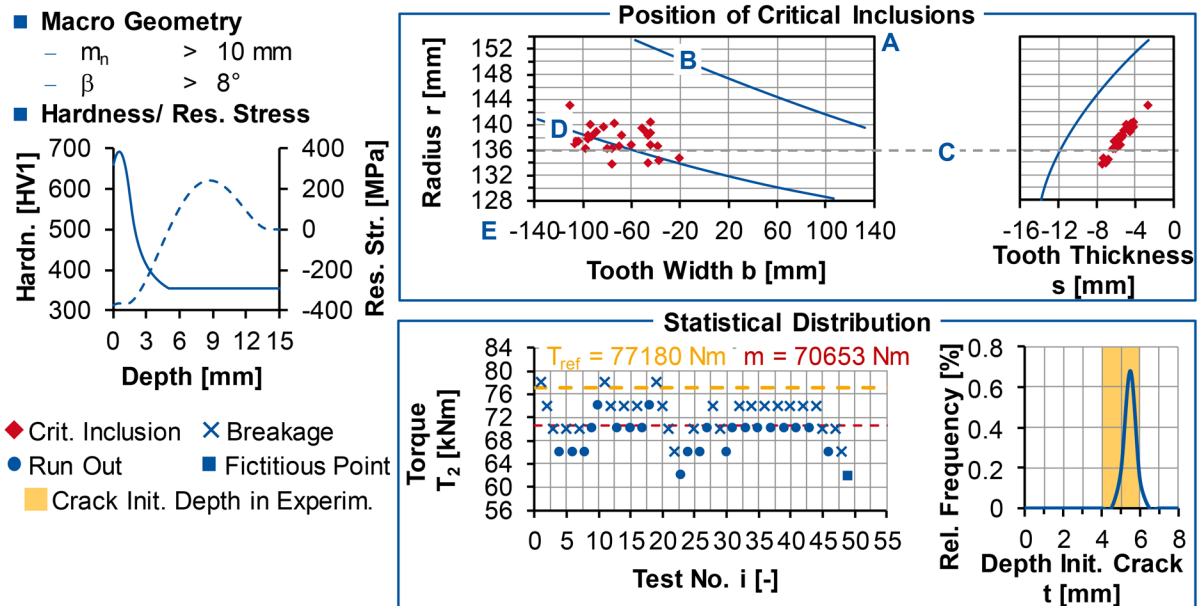
experimental determination of the load capacity up to a maximum torque  $T_{\text{max}} = 5,000 \text{ Nm}$  at a maximum rotational speed  $n_{\text{max}} = 3,400 \text{ min}^{-1}$ . Therefore, an injection lubrication is recommended for the experiments. In order to enable a classification to the state of the art, the investigations were carried out at a rotational speed of  $n_{\text{Test}} = 2,600 \text{ min}^{-1}$ . The lubricant used is the common oil for load capacity investigations FVA3 +4% Anglamlol. The oil temperature was defined to  $T_{\text{Oil}} = 60^\circ\text{C}$  with a flow rate of  $V_{\text{Oil}} = 5 \text{ l/min}$ . The direction of rotation of the motor and the direction of torque applied were selected in a way that the pinion drives the counter gear. According to the state of the art, an estimated maximum torque of  $T_{\text{max}} \approx 3,500 \text{ Nm}$

- **Macro Geometry**
    - $m_n$  = 8 mm
    - $z_{1/2}$  = 24/25
    - $b_{1/2}$  = 18/18 mm
    - $\alpha_n$  = 20°
    - $\beta$  = 0°
  - **Micro Geometry**
    - $C_{\alpha a}$  = 75±5 μm
  - **Hardness/Res. Stress**
- 
- ◆ Crit. Inclusion
  - × Breakage
  - Run Out
  - Fictitious Point
  - Crack Init. Depth in Experim.



© WZL

Figure 7 Comparison TFF Endurance Limit between Experiment and Simulation.



© WZL

Figure 8 Comparison TFF Endurance Limit between Operation Torque and Simulation.

is applicable for the test gear geometry. The test rig therefore has enough power reserve to react to unexpected test results in order to enable tests at higher torques. [Ref. KONO18]

### 5.1.2. Results

The endurance strength is determined using the staircase method and extended IABG evaluation method according to HÜCK [Ref. HÜCK83]. The results are illustrated in Figure 6. In the lower part of Figure 6, the tests to determine the endurance strength are supplemented by the fictitious point and evaluated using the staircase method. In total, 8 test points (including the fictitious point) could be evaluated. The result is an endurance strength torque limit of  $T_{1,End.} = 2,250 \text{ Nm}$  at a failure probability of  $P_A = 50\%$ .

The teeth fail in the range of finite life due to tooth flank fractures. This damage mechanism also limits the previously determined endurance strength, as it can be seen in the upper part of Figure 6 in the SN-Curve. However, one test with a driving torque of  $T_1 = 3,200 \text{ Nm}$  was stopped with a pitting damage. Consequently, the load capacity limits for pitting and tooth flank fracture damage are close. The tests carried out show a low scatter, which is visible in the SN-Curve. Only one test with driving torque  $T_1 = 2,200 \text{ Nm}$  has a reduced number of load cycles. Since the test was used to evaluate the endurance strength, for which the number of load cycles is irrelevant, the result can be classified as valid.

Figure 7 illustrates the results of the tooth flank fracture load capacity calculation as well as the comparison between simulative and experimental determined endurance strength. The damage causing material inhomogeneities are located in the area of the single tooth contact close to the diameter of the lower transition point B. Due to the symmetric load on the spur gear, all critical inhomogeneities are in the center of the tooth in lead direction. With regard to the depth of crack initiation, the maximum relative frequency is in the range of  $t = 2 \dots 2.5 \text{ mm}$ . This

corresponds to the depth of the crack initiation points discovered in the metallographic analysis [Ref. KONO18].

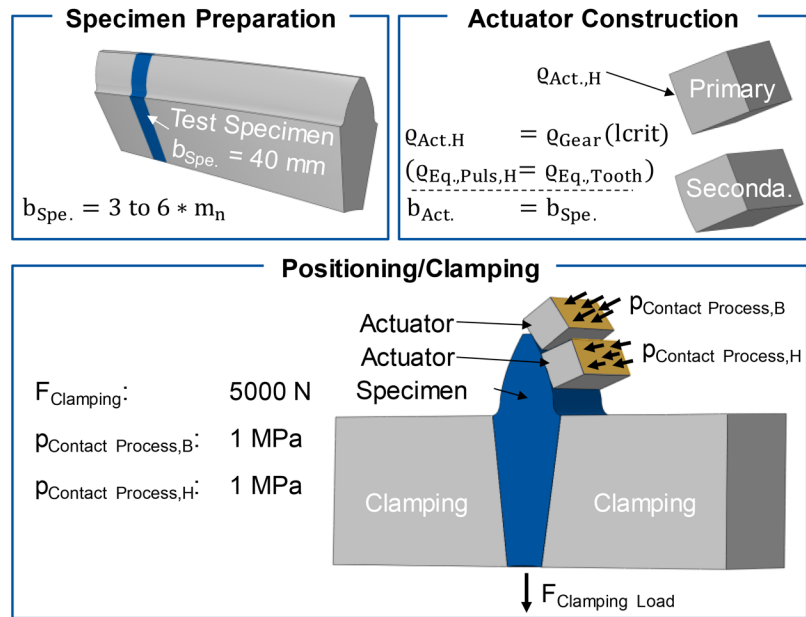
The evaluation of the simulative staircase procedure is carried out based on 35 simulation points. The mean value of the endurance torque is determined to  $T_{1,End.} = 2,266 \text{ Nm}$ . The tests spread over three load values between  $T_1 = 2,000 \text{ Nm}$  and  $T_1 = 2,400 \text{ Nm}$ , resulting in a standard deviation of  $s = 126.5 \text{ Nm}$  respectively  $s = 5.6\%$ . In comparison to the experimentally determined endurance strength, the difference is  $\Delta T_{1,End.} = 1\%$ , which is lower than the standard deviation.

### 5.2 Simulation of Gear Set from Industrial Application (Wind Turbine)

In addition to the experimental validation on the back-to-back test rig, a large-modulus helical gear from a wind turbine which showed tooth flank fractures during operation, was recalculated using the developed calculation approach by KONOWALCZYK [Ref. KONO18]. The shared geometry data is subject to confidentiality and cannot be published in this report. The normal module is  $m_n > 10 \text{ mm}$  and the helix angle is  $\beta > 8^\circ$ . The material is case-hardened 18CrNiMo7-6 with a surface hardness  $HV_s = 660 \text{ HV1}$ , a case hardening depth  $CHD_{50} = 1.64 \text{ mm}$  and a core hardness  $HV_c = 355 \text{ HV1}$ . In application the counter gear drives and the pinion is driven.

The calculation results are shown in Figure 8. The critical inhomogeneities leading to tooth flank fracture are mainly located on the left gear side in the transition between the double and triple tooth contact. In this area of the tooth flank there is a high stress due to contact pressure on the one hand and a high bending stress due to high loads on higher diameters on the other hand. The statistical evaluation shows that the majority of critical inhomogeneities are in a depth between  $t = 4 \dots 6 \text{ mm}$ . This corresponds to observations made in industrial practice. The evaluation of the simulative staircase procedure results in an endurance strength torque of  $T_2 = 70,653 \text{ kNm}$ .

- **Material Properties**
  - $E_{\text{Actuator}} = 210000 \text{ MPa}$
  - $\nu_{\text{Actuator}} = 0.3$
  - $E_{\text{Clamp}} = 210000 \text{ MPa}$
  - $\nu_{\text{Clamp}} = 0.3$
- **Key**
  - $b$ : Width
  - $B$ : Bending
  - $H$ : Hertzian Cont.
  - $l_{\text{crit}}$ : Critical Cont. Line
  - $m_n$ : Normal Module
  - $p$ : Pressure
  - $\rho$ : Curvature Radius
  - $\text{Act.}$ : Actuator
  - $\text{Eq.}$ : Equivalent Curvat.
  - $\text{Puls.}$ : Pulsator Contact
  - $\text{Spe.}$ : Test Specimen
  - $\text{Tooth.}$ : Tooth Contact



© WZL

**Figure 9 Construction of Simulation Model.**

The tests spread over a torque range between  $T_2 = 62 \text{ kNm}$  and  $T_2 = 78 \text{ kNm}$ . A total of 48 simulations could be evaluated, which results in a standard deviation of  $s = 3.8 \text{ kNm}$  or  $s = 5.4\%$ . [Ref. KONO18].

Compared to the nominal operating torque ( $T_2 = 77,180 \text{ kNm}$ ), the calculated endurance torque is  $\Delta T_2 = 8.5\%$  lower, which corresponds to the observations made in operation, where several tooth flank fractures occurred. The calculated crack initiation depth and position is also correlating to the observations, where the crack origin was located in  $t \approx 5 \text{ mm}$  depth in the transition point between triple and double tooth contact shifted to the left of the tooth center in lead direction. [Ref. KONO18].

## 6/ Analogy Test Concept

In order to economically test the tooth flank fracture load capacity of large-modulus gears in an analogy test rig, KONOWALCZYK developed a double pulsator concept which is able to apply stresses caused by HERTZIAN contact and bending, cf. Figure 2 [Ref. KONO18]. In Chapter 6, a method to determine the load sequences of the actuators is presented which allows to induce equal stresses in the point of interest (POI) as in the running test. The newly developed method is applicable for spur and helical gears. The simulated test gear in Chapter 6 is the tooth flank fracture critical pinion which is also analyzed in Chapter 5.2. The point of interest defined is the center of all calculated crack initiation points according to the calculation approach presented in Chapter 4, Figure 8.

### 6.1 Simulation Model and Pulsator-Load Definition

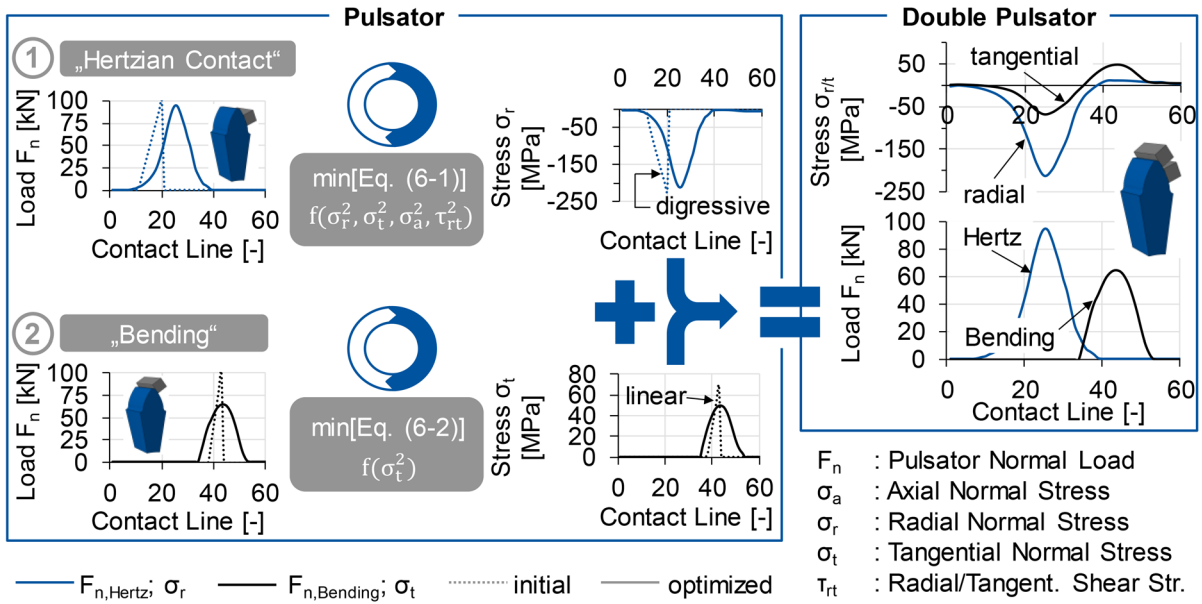
The simulations presented in this report were performed in the software *Abaqus/CAE* 6.14-6. The simulation model was set up in three steps, Figure 9. In the first step, a tooth of the test gear was extracted from the gear mesh which was implemented in the tooth contact simulation software “*FE-Stirnradkette*”

(STIRAK).

In order to enable an analogy study using the pulsator principle, the TFF critical part of the tooth in lead direction determined from field observations and according to the calculation by KONOWALCZYK was virtually separated, Figure 9 [Ref. KONO18]. In accordance with STAHL ET AL. a width of the test specimen in the range  $3 \cdot m_n \leq b \leq 6 \cdot m_n$  was defined [Ref. Ref. STAHL12]. In the second step, the two actuators were designed. To achieve a line contact between the two actuators and the test specimen over the entire width, the width of the actuators correspond at least to the width of the test specimen. In order to obtain an equal local material strain in the TFF critical volume, the equivalent curvature radius in the line contact between primary actuator and test specimen has to be analogous to the equivalent radius of curvature in the contact pinion/ counter gear. Consequently, the radius of curvature of the primary actuator has to correspond to the radius of curvature of the counter gear at the TFF critical contact line ( $\rho_{\text{act.,H}} = \rho_{\text{rad}}(l_{\text{crit}})$ ), Figure 9.

The aim of the load-sequence optimization is an analogue local material strain in the evaluation point (point of interest, POI) between running and analogy test. The running test respectively the real tooth contact is realized by a quasi-static rolling-sliding simulation over three base-pitches. The target value is the stress tensor sequence of the simulated tooth contact in the POI. The procedure of the method is shown in Figure 10.

The first step is the optimization of the HERTZIAN contact, which is imitated by the primary actuator. The contact between the primary actuator and the tooth flank is initially loaded with a load ramp within the limits of the actuator’s performance, Fig. 10. The secondary actuator is load-free during the optimization of the HERTZIAN contact. The results of the initial load ramp are stress tensors in the POI as a function of the simulated load levels. Based on the digressive relationship between pulsator load and resulting stress tensor at the POI, all stresses at the



© WZL

Figure 10 Method for the Optimization of the Pulsator Load.

POI can be interpolated to any load within the load ramp out of the initial load.

In order to optimize the load sequence, the quadratic minimization function is defined according to Equation (6-1). The function is based on the difference of all relevant stress components between analogy test and running test. The relevant stress components are all normal stresses and the shear stress in the radial/tangential plane. The two remaining shear stresses are not considered in the optimization function due to their low stress value. The relevant stress components are set in relation to the highest occurring stress (usually radial compressive normal stress). Additionally, weighting constants (A-C) are introduced to be able to weight individual stress components more strongly. The weighting constants are the result of a variation calculation and can be adapted to the specific gear set. Whether the selected weighting constants can be transferred to other gear geometries has to be checked in future work. The optimization algorithm uses the determined interpolation functions and iterates the pulsator load until the quadratic minimization function reaches the smallest possible value.

$$F = (\sigma_{t,real} - \sigma_{t,puls,Bending} - \sigma_{t,puls,Hertz})^2 + \left( A \times \frac{\max |\sigma_{r,real}|}{\max |\sigma_{t,real}|} \right)^2 (\sigma_{t,real} - \sigma_{t,puls,Hertz})^2 + \left( B \times \frac{\max |\sigma_{r,real}|}{\max |\sigma_{a,real}|} \right)^2 (\sigma_{a,real} - \sigma_{a,puls,Hertz})^2 + \left( C \times \frac{\max |\sigma_{r,real}|}{\max |\tau_{rt,real}|} \right)^2 (\tau_{rt,real} - \tau_{rt,puls,Hertz})^2$$

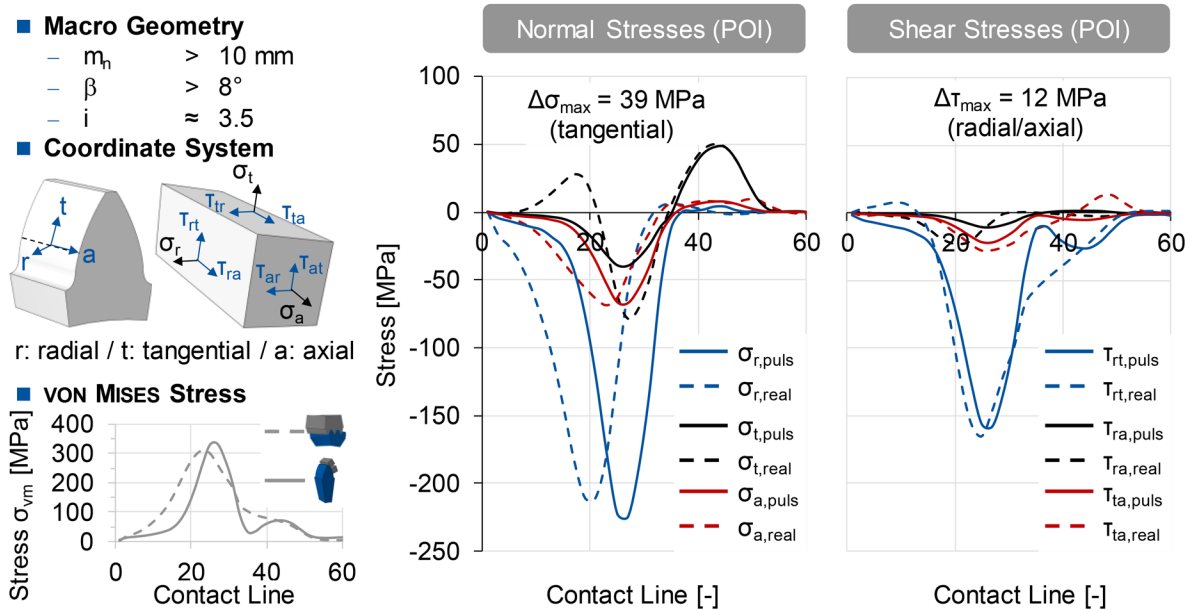
A-C	[-]	Weighting Constants
F	[-]	Target Function
$\sigma$	[MPa]	Normal Stress
$\tau$	[MPa]	Shear Stress
a:		Axial
r:		Radial
t:		Tangential
Hertz:		Hertzian Contact/ Primary Actuator

puls: Pulsator  
 real: Tooth Contact

The first optimization algorithm provides pulsator load-sequences and their associated stress tensors for the primary actuator (Pulsator 1, HERTZIAN Contact). The procedure for optimizing the pulsator loads of the secondary actuator is analogous to the optimization of the primary actuator, whereby a different minimization function is used as a basis, Fig. 10. Since there is a linear relationship between the pulsator load at the secondary actuator and the stress at the POI (bending beam theory), a simulation at maximum load at the secondary actuator with subsequent linear interpolation is sufficient. The function only considers the normal stress in the tangential direction, since this stress component is the largest driver of the secondary stress mainly caused by bending, Equation (6-2). With the analogy test rig, it is intended that both actuators can apply load simultaneously in order to enable a smooth transition between primary and secondary stress. This is also considered in the simulation by superposition of the stresses from the optimization of the HERTZIAN contact in the downstream minimization function. In the last step, the pulsator load and stress tensor sequences of both optimization steps are merged. The validation of the determined stress tensor sequence is carried out by a final FE simulation with the calculated pulsator load sequences and subsequent comparison with the quasi-static rolling-sliding simulation.

$$F = (\sigma_{t,real} - \sigma_{t,puls,Bending} - \sigma_{t,puls,Hertz})^2 \quad (6-2)$$

F	[-]	Target Function
$\sigma$	[MPa]	Normal Stress
t:		Tangential
Bending:		Secondary Actuator
Hertz:		Hertzian Contact/ Primary Actuator
puls:		Pulsator
real:		Tooth Contact



© WZL

Figure 11 Stress Tensor Sequence, Comparison Real Tooth Contact/ Analogy Concept.

## 6.2 Stress Comparison between Analogy Concept and Real Tooth Contact

A detailed comparison of all stress components at the POI between the running test and the analogy test is shown in Figure 11. The comparison of the normal stress amplitudes at the POI shows that the maximum magnitude of all stress component amplitudes can be reproduced by the analogy test rig. In particular, the radial compressive stress  $\sigma_r$  due to the HERTZIAN contact, the axial compressive stress  $\sigma_a$  due to the HERTZIAN contact as well as the tangential tensile stress  $\sigma_t$  due to bending can be reproduced in the analogy test. However, there are also deficits due to the stationary positioning of the primary actuator. On the one hand, the tangential tensile stress upstream of the tangential compressive stress  $\sigma_t$  differs because it results from the rolling-sliding contact. An additional actuation of the secondary actuator would be conceivable at this point, but a tangential tensile stress with higher amplitude is induced at a later point in time by the secondary stress anyway. It can be assumed that the upstream tangential tensile stress has a negligible influence on the damage behavior.

On the other hand, the highest amplitudes of the stress components are present at the same time in the analogy test, while the highest amplitudes follow one another in the running test. For this reason, it will also not be possible with the analogy concept presented to exactly reproduce the maximum amplitudes of all normal stress components. By introducing weighting constants in Equation (6-1), an approximation of the tangential compressive stress  $\sigma_t$  to the running test can be achieved. On the other hand, it is visible in the normal stress sequences (Fig. 11) that a higher radial compressive stress  $\sigma_r$  is reached than in the running test. Accordingly, a stronger weighting of the tangential stress  $\sigma_t$  simultaneously leads to higher radial and axial compressive stresses than in the running test. The VON MISES equivalent stress (see Fig. 11, diagram bottom left) shows that there is

no significant change in the equivalent stress between the analogy test and the running test despite the time displacement of the stress amplitudes. This is an indicator that no significant change in fatigue behavior is expected from the stationary load application. However, a precise check has to be carried out in experimental analogy investigations. The sequences of the shear stresses at the POI can also be reproduced in the analogy test (Fig. 11, right diagram.) The amounts of all shear stress components are lower in the analogy test than in the running test, whereby the difference for all three shear stress components is  $\Delta\tau \leq 12 \text{ MPa}$ . In particular, the shear stress in the radial/tangential plane  $\tau_{rad/tan}$ , which KONOWALCZYK can only reproduce to a limited extent, shows a better correlation between the analogy test and the running test due to the adjusted primary actuator position and the developed optimization method.

## 7. Summary and Outlook

The present report deals with the development and validation of a calculation approach for tooth flank fracture load capacity of large-modulus spur and helical gears as well as the development of an analogy test rig for the economic investigation of tooth flank fractures. Currently existing calculation approaches do not sufficiently capture individual influencing parameters on the tooth flank fracture load capacity (possible residual tensile stresses in the core, exact local stress sequence caused by HERTZIAN contact and bending, crack causing material inhomogeneities). For this reason, a method was developed at WZL based on a statistically material inhomogeneity-based approach and the calculation of local material strains, which enables the calculation of a virtual staircase procedure with evaluation of an average endurance strength and a standard deviation [Ref. KONO18]. The method could be validated on the basis of experimental investigations on a large-modulus spur gear ( $m_n=8 \text{ mm}$ ,  $z_2=24/25$ ,  $\beta=0^\circ$ ) as well as on the basis of a tooth

flank fracture-critical gear from a wind turbine ( $m_n > 10 \text{ mm}$ ,  $\beta > 8^\circ$ ). The calculated endurance strengths as well as the calculated initial crack locations correlate with the observations from the experiment and practice.

The concept of a double pulsator was developed for the economic investigation of the tooth flank fracture load capacity of large gears in an analogy test. With the developed concept it is possible to reproduce the stress sequence in the tooth flank fracture critical volume of the gear (point of interest). In this report, a method is presented which allows to determine the pulsator load sequences automatically in order to generate an equal stress state between analogy and running test. Thus, gears can efficiently be investigated with regard to tooth flank fracture load capacity, similar to the classical pulsator concept for the investigation of tooth root load capacity.

In future work, a validation of the method by means of recalculating several gear geometries will be focused. In addition, a sensitivity analysis of the calculation approach on the basis of different gear geometries will be carried out to analyze the influencing parameters on the tooth flank fracture load capacity. Within the framework of the DFG research project BR 2905/90-1 the developed analogy test rig is designed and put into operation. Subsequently, first tests with focus on tooth flank fracture generation are carried out on the gear geometries presented in this report.

#### Acknowledgement



The authors gratefully acknowledge financial support by the German Research Foundation (DFG) [BR 2905/90-1] for the achievement of the project results.



The authors gratefully acknowledge financial support by the Research Association for Power Transmission Engineering (FVA) [FVA 695] for the achievement of the project results.

#### References

- [ANNA03] Annast, R. "Kegelrad-Flankenbruch," Diss. TU München, 2003.
- [BREC17] Brecher, C., C. Löpenhaus and J. Pollaschek. "Automated Defect Size Determination for Gear Tooth Root Bending Strength Simulation," In: *WIT Transactions of Engineering Sciences*, 2017, Nr. 116, S. 87–97.
- [BRUC06] Bruckmeier, S. "Flankenbruch bei Stirnradgetrieben," Diss. TU München, 2006.
- [FKM03] Richtlinie FKM (2003). Rechnerischer Festigkeitsnachweis für Maschinenbauteile.
- [HENS15] Henser, J. "Berechnung der Zahnfußtragfähigkeit von Beveloidverzahnungen," Diss. RWTH Aachen University, 2015.
- [HÜCK83] Hück, M. "Ein verbessertes Verfahren für die Auswertung von Treppenstufenversuchen," In: *Werkstofftechnik*, 24. Jg., 1983, S. 406–417.
- [ISO19] Norm ISO/TS 6336. Part 4 (January 2019) Calculation of load capacity of spur and helical gears - Part 4: Calculation of tooth flank fracture load capacity.
- [KLOC18] Klocke, F., C. Löpenhaus and P. Konowalczyk. Einfluss des Abschleißbetrags auf die Zahnflankentragfähigkeit großmoduliger einsatzgehärteter Zahnradern, Forschungsvereinigung Antriebstechnik e.V., Frankfurt a.M., 2018.
- [KONO18] Konowalczyk, P. "Grübchen- und Zahnflankenbruchtragfähigkeit großmoduliger Stirnräder. Einfluss von Werkstoffreinheitsgrad, Härte- und Eigen- spannungstiefenverlauf," Diss. RWTH Aachen, 2018.
- [LANG79] Lang, O.-R. "Dimensionierung komplizierter Bauteile aus Stahl im Bereich der Zeit- und Dauerfestigkeit," In: *Werkstofftechnik*, 10. Jg., 1979, S. 24–29.
- [LEIM19] Leimann, D. and W. Smet. "Calculation of Tooth Flank Fracture Load Capacity acc. to the method of Leimann," In: *Tagungsband zur Conference for Wind Power Drives*, Aachen, 12./13.03.2019, 2019, S. 05/1–11.
- [LIU91] Liu, J. "Beitrag zur Verbesserung der Dauerfestigkeitsberechnung bei mehr-achsiger Beanspruchung," Diss. TU Clausthal, 1991.
- [LOEP15] Löpenhaus, C. "Untersuchung und Berechnung der Wälzfestigkeit im Scheiben- und Zahnflankenkontakt," Diss. RWTH Aachen University, 2015.
- [MEIS19] Meis, J.-A. "Flank fracture assessment of planet gears." In: *Tagungsband zur Conference for Wind Power Drives*, Aachen, 12./13.03.2019, 2019, S. 03/1–12.
- [MURA02] Murakami, Y. "Metal fatigue. Effects of small defects and nonmetallic inclusions," 1. Aufl. Amsterdam: Elsevier, 2002.
- [OCTR18] Octrue, M., D. Ghribi and P. Sainsot. "A Contribution To Study The Tooth Flank Fracture (TFF) In Cylindrical Gears," In: *Procedia Engineering*, 2018, Nr. 213, S. 215–226.
- [PATE16] Al, B., R. Patel and P. Langlois. "Finite Element Analysis of Tooth Flank Fracture Using Boundary Conditions from LTCA," In: *Gear Technology*, 2016, S. 62–68.
- [POPO10] Popov, V. *Kontaktmechanik und Reibung. Von der Nanotribologie bis zur Erdbebendynamik*. Berlin: Springer, 2010.
- [STAH12] Stahl, K., T. Tobie and P. Matt. "Empfehlungen zur Vereinheitlichung von Tragfähigkeitsversuchen an vergüteten und gehärteten Zylinderrädern." FVA Merkblatt auf Basis von FVA-Merkblatt 0/5 und FVA 563 I, Forschungsvereinigung Antriebstechnik e.V., Frankfurt a.M., 2012.
- [TOBI01] Tobie, T. "Zur Grübchen- und Zahnfußtragfähigkeit einsatzgehärteter Zahnradern. Einflüsse aus Einsatzhärtungstiefe, Wärmebehandlung und Fertigung bei unterschiedlicher Baugröße," Diss. TU München, 2001.
- [WEBE15] Weber, R. "Auslegungskonzept gegen Volumenversagen bei einsatzgehärteten Stirnrädern," Diss. Universität Kassel, 2015.
- [WICK17] Wickborn, C. "Erweiterung der Flankentragfähigkeitsberechnung von Stirnrädern in der Werkstofftiefe - Einfluss von Werkstoffeigenschaften und Werkstoffdefekten," Diss. TU München, 2017.
- [WITZ12] Witzig, J. "Flankenbruch - eine Grenze der Zahnradtragfähigkeit in der Werkstofftiefe," TU München, 2012.

**Prof. Dr.-Ing. Christian Brecher** has since January 2004 been Ordinary Professor for Machine Tools at the Laboratory for Machine Tools and Production Engineering (WZL) of the RWTH Aachen, as well as Director of the Department for Production Machines at the Fraunhofer Institute for Production Technology IPT. Upon finishing his academic studies in mechanical engineering, Brecher started his professional career first as a research assistant and later as team leader in the department for machine investigation and evaluation at the WZL. From 1999 to April 2001, he was responsible for the department of machine tools in his capacity as a Senior Engineer. After a short spell as a consultant in the aviation industry, Professor Brecher was appointed in August 2001 as the Director for Development at the DS Technologie Werkzeugmaschinenbau GmbH, Mönchengladbach, where he was responsible for construction and development until December 2003. Brecher has received numerous honors and awards, including the Springorum Commemorative Coin; the Borchers Medal of the RWTH Aachen; the Scholarship Award of the Association of German Tool Manufacturers (Verein Deutscher Werkzeugmaschinenfabriken VDWM); and the Otto Kienzle Memorial Coin of the Scientific Society for Production Technology (Wissenschaftliche Gesellschaft für Produktionstechnik WGP).



**Dr.-Ing. Dipl.-Wirt.-Ing. Christoph Löpenhaus**

is since 2021 working with Flender GmbH as head of production for the part manufacturing plants in Bocholt and Voerde, Germany. Flender is a worldwide leading provider of drive systems especially for wind turbine and industry applications. From 2019-2021 he was Business Development Manager Geared Bearings at Cerobear GmbH, a leading manufacturer of hybrid bearings especially in the aerospace, space, and industry segment. From 2014–2019 he held the position as Chief Engineer of the Department of Gear Technology of WZL, RWTH Aachen with research focus on gear manufacturing, design, and testing. He previously worked with WZL as Team Leader and Research Assistant. His educational background is in the field of Industrial Engineering with a diploma in 2009 and a Ph.D. in mechanical engineering in the field of gear technology in 2015. For his scientific achievements he was awarded the Springorum Commemorative Coin in 2010 and the Borchers Badge in 2016.



**Fabian Goergen** studied mechanical engineering at RWTH Aachen University. He has bachelor of science and masters degrees in production engineering. He is a research assistant, Laboratory for Machine Tools and Production Engineering (WZL) at RWTH Aachen University (Gear Department), with a focus on Gear Power Density.



# GOTTA GET BACK IN TIME...



It may not be as impressive as a DeLorean, but if time travel is your thing we have you covered at

WWW.  
**geartechnology**  
.com.

Today, our user-friendly archive (1984 to present) is now available online with an optimized search engine that allows subscribers to locate specific articles using keywords and phrases.

We've created a database where subscribers can peruse more than thirty-five years of gear manufacturing articles without leaving their desks.

In an era where content is king. let *Gear Technology* be your destination for the past, present and future of gear manufacturing.

**[www.geartechnology.com/issues](http://www.geartechnology.com/issues)**

For Related Articles Search

tooth flank fracture 

at [www.geartechnology.com](http://www.geartechnology.com)